0026-895X/08/7304-1092–1104$20.00
MOLECULAR PHARMACOLOGY

Mol Pharmacol 73:1092–1104, 2008

Vol. 73, No. 4
43042/3320955
Printed in U.S.A.

Wide Turn Diversity in Protein Transmembrane Helices Implications for G-Protein-Coupled Receptor and Other Polytopic Membrane Protein Structure and Function[S]

R. Peter Riek, Angela A. Finch, Gillian E. Begg, and Robert M. Graham

Computational and Structural Biology Division (R.P.R.) and Molecular Cardiology (A.A.F., G.B., R.M.G.) Divisions, Victor Chang Cardiac Research Institute, Darlinghurst, New South Wales, Australia; and Department of Pharmacology, School of Medical Sciences, University of New South Wales, Kensington, New South Wales, Australia (A.A.F.)

Received October 30, 2007; accepted January 17, 2008

ABSTRACT

Previously, we showed that perturbations of protein transmembrane helices are manifested as one of three types of noncanonical structures (wide turns, tight turns, and kinks), which, compared with α-helices, are evident by distinctive $C\alpha_i \rightarrow C\alpha_x$ distances. In this study, we report the analysis of more than 3000 transmembrane helices in 244 crystal structures from which we identified 70 wide turns (29 proline- and 41 non–proline-induced). Based on differences in the $C\alpha_i \rightarrow C\alpha_{i-4}$ and $C\alpha_i \rightarrow C\alpha_{i-5}$ profiles, we show that wide turns can be subclassified into three distinct subclasses (W_1, W_2, and W_3) that differ with regard to the number and position of backbone $i \rightarrow i-5$ H-bonds formed N-terminal to the perturbing or signature proline or nonproline residue. Although wide turns generally produce changes in helical direction of 20° to 30° and a lateral shift in the helical axis, some of the W_3 subclass are associated with changes of $<5°$. We also show that the distinct architectural features of wide turns allow the carbonyl bond of the *i−4th* residue, which is located on the widened loop of a wide turn, to be directed away from the helical axis. This provides regions of flexibility within helical regions allowing, for example, unique opportunities for interhelical H-bonding, including interactions with glycine zipper motifs, and for ion and cofactor binding. Furthermore, differences in wide-turn subtype usage by related protein family members, such as the G-protein-coupled receptors rhodopsin and the β2-adrenergic receptor, can significantly affect the orientation and position of residues critical for ligand binding and receptor activation.

More than 70% of helices in proteins are curved or contain one or more kinks or other non-α-helical structures (e.g., π-bulges, 3_{10}-helices, kinks) (Barlow and Thornton, 1988; Bansal et al., 2000). This is particularly the case for polytopic transmembrane proteins, such as G-protein-coupled receptors and ion channels, the relatively long transmembrane helices of which—straight, curved, or kinked—pack into compact elliptical or circular domains to form ligand binding pockets, or channels for the passage of ions. These noncanonical structures or deviations in α-helicity that are due to the perturbing effects of both prolyl and nonprolyl residues, identified here as the *signature* residue, are contained within one to two turns of a helix. They change the pitch of the helix and displace backbone atoms of involved residues from the positions they would normally occupy in an α-helical structure. Using methods that reveal details about the shape of the helix, we previously identified three types of noncanonical structures: wide turns, tight turns, and kinks. In particular, we showed that noncanonical structures could be discerned from $C\alpha_i \rightarrow C\alpha_x$ distance-difference plots [that is, plots of the differences between the $C\alpha_i \rightarrow C\alpha_x$ distances ($x = -2 \rightarrow -5$) of residues forming the noncanonical regions, and those of a regular α-helix] (Riek et al., 2001).

These $C\alpha_i \rightarrow C\alpha_x$ distance-difference plots reveal alterations in regular α-helical geometry because, although peptide bond lengths are essentially invariant and the distance between $C\alpha$ atoms of adjacent residues remains constant, rotations about the bonds on either side of the $C\alpha$ atom of each residue produce changes in the ϕ and ψ dihedral angles, leading to altered distances between $C\alpha$ atoms two or more residues apart. As a result, non–α-helical regions are evident as positive or negative deviations in the distances between $C\alpha$ atoms two to five residues apart in sequence, compared with the equivalent residues in an α-helix (Riek et al., 2001; Rigoutsos et al., 2003) (Supplemental Fig. 1).

Although $C\alpha_i \rightarrow C\alpha_x$ distance-difference plots allow wide

Supported in part by grant 354400 from the National Health and Medical Research Council, Australia.
Article, publication date, and citation information can be found at http://molpharm.aspetjournals.org.
doi:10.1124/mol.107.043042.
[S] The online version of this article (available at http://molpharm.aspetjournals.org) contains supplemental material.

ABBREVIATIONS: RC, reaction center; BCCO, bovine cytochrome *c* oxidase; AR, adrenergic receptor; TM, transmembrane domain.

turns, tight turns, and kinks to be identified, neither such plots nor other analyses of helical architecture provide sufficient detail to fully characterize noncanonical regions. For example, Sugeta and Miyazawa (1967) and others (Aqvist, 1986; Christopher et al., 1996; Bansal et al., 2000; Visiers et al., 2000; Cordes et al., 2002; Bright and Sansom, 2003; Mohapatra et al., 2004; Lopera et al., 2005) determined the helical axis, the bend angle of the helix, the rise per residue, and the inter-residue angle, by "best-fitting" the helical regions to a canonical four residue α-helical template with the use of a centroid calculation (involving four consecutive Cα atoms) or a least-squares procedure, which involves one to two turns of helix either side of the bend created by a noncanonical segment, to calculate the bend angle. These approaches suffer from an inability to evaluate helical geometry on a residue-to-residue basis. Moreover, noncanonical segments, such as wide turns, involve an eccentric enlargement of the helical diameter, resulting in lateral displacement of the helical axis. This behavior is not accurately modeled using available methods, which rather, artifactually skew and twist the helical axis. Other approaches to identify helical perturbations that result in wide turns, also called π-bulges, require the presence of one or more π ($i \rightarrow i-5$) hydrogen-bonds (H-bonds) (Kabasch and Sander, 1983; Richards and Kundrot, 1988; Frishman and Argos, 1995; Labesse et al., 1997; Weaver, 2000; Fodje and Al-Karadaghi, 2002) and a turn of α-helix before and after the wide turn (Cartailler and Luecke, 2004). As a result, wide turns not bounded by complete α-helical turns may not be identified.

As we show here, these shortcomings can be obviated by calculating the change in helical direction on a residue-to-residue basis. This allows the effects of the signature residue and other residues within a noncanonical region, to be accurately determined. Using this approach, we have identified three distinct wide-turn types in transmembrane protein helices—unique architectural features that provide opportunities for hydrogen-bonding interactions with adjacent helices, or for ion or cofactor binding.

Materials and Methods

Database and Identification of Helices. Transmembrane helical regions were identified using Insight II (Accelrys, San Diego, CA). To determine potential H-bonding interactions typical of a 3_{10}-helix ($i \rightarrow i-3$), α-helix ($i \rightarrow i-4$), or π-helix ($i \rightarrow i-5$), hydrogen atoms were added either at pH 7.0 or at the pH specified in the structure file.

We treated the same proteins from different species as separate examples, if they display sequence differences in the noncanonical structures. Some proteins are highly represented with multiple entries in the database, particularly structures for photosynthetic reaction centers and bacteriorhodopsin. Initially, we considered all such entries if the resolution criteria were met (resolution, $\leq$3.0 Å; R-value, $\leq$0.3). However, if the structures of the transmembrane helices were identical in the various entries, only one representative member was evaluated. In instances in which structural variations were evident between entries for the same protein as a result of differences in crystallization conditions, to the different mutant forms, or different functional states (e.g., oxidized or reduced) or to crystallization in the presence or absence of different inhibitors or different metal ions, all such entries were considered in evaluating the detailed geometry of wide turns.

Identification of Noncanonical Regions. Noncanonical segments were identified based on C$\alpha_i \rightarrow$Cα_x distance-difference plots (Supplemental Table 1), as described previously (Riek et al., 2001). Here we focus on the wide turn or π-bulge category of noncanonical structures, which display Cα_{i-2} and Cα_{i-3} distance differences that are positive and Cα_{i-4} and Cα_{i-5} distance differences that are negative.

In noncanonical helical regions with proline as the helix-perturbing residue, the position containing the proline is designated as the signature residue position (S_0). Nonprolyl residues that disrupt α-helical geometry result in C$\alpha_i \rightarrow$Cα_x distance-difference profiles similar to those produced by prolyl residues (Supplemental Fig. 1, D–F). In such instances, these nonprolyl residues are the signature residues. Thus, such nonprolyl residues are defined as the signature residue if their substitution by a proline would produce a similar C$\alpha_I \rightarrow$Cα_x profile.

Helical Parameters. The effects of the residues within a noncanonical region on helical structure can be seen from changes in the position and direction of the helical axis. To accurately determine such changes, we characterized transmembrane protein helices on a residue-to-residue basis. This was done by evaluating helical parameters that are based on the coordinates of the atoms forming each C$\alpha_i \rightarrow$Cα_{i+1} segment. From these coordinates, nine parameters could be determined: the three backbone dihedral angles, ϕ, ψ, and ω; the three bond lengths; and the three bond angles of the backbone atoms. These parameters alone allow a helical segment of as little as four residues to be constructed. The regularity of such a four-residue helix enables other helical parameters to be calculated, including the helical spoke angle, the radius of the helical segment, and the direction and length (rise per residue) of the helical axis (Riek et al., 2001). Based on these considerations, to determine the helical axis for any residue-to-residue pair, we constructed a de novo computed four-residue helix using the parameters determined from the particular C$\alpha_i \rightarrow$Cα_{i+1} segment being examined (Supplemental Fig. 2). The regularity of such de novo constructed helices enabled precise trigonometrical determination of the positions of two helical axis points

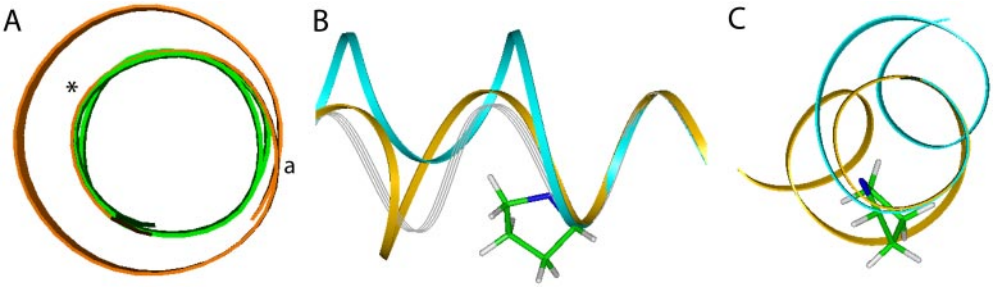

Fig. 1. Ribbon traces showing paths of wide turns and an α-helix. A, an α-helix and W_3 wide turn induced by prolines viewed along the helical axis from C to N terminus. This wide turn example has <5° change in direction. a, position at which the widened turn of the helix starts and then resumes α-helical geometry one full turn further N-terminal. The position of the pyrrolidine ring is indicated by an asterisk. Green ribbon: α-helix; orange ribbon: wide turn. B, the yellow ribbon shows the path of a W_1 wide turn looping out and around the pyrrolidine ring. The gray lines show the path of an α-helix. The path of a wide turn formed by a partial unwinding of the helix is indicated by the cyan ribbon. C, view of B rotated by 90° showing the divergent paths of these wide turns. (Gray ribbon not shown.)

for each four-residue helix. The helical axis vector, which is equivalent to the rise per residue for each $C\alpha_i \rightarrow C\alpha_{i+1}$ segment within the helical region of interest (Supplemental Data, Fig. 2C), was determined from the helical axis points. The vector of the helical axis indicates the helical path of a segment and is defined in terms of its direction, position, and length.

The helical bend angle is the change in helical direction resulting from the effect of the signature residue on helical structure. This was determined by calculating the angle between the axis vectors of the S_0-S_1 and S_{-7}-S_{-6} segments. The S_0-S_1 segment (designated as the reference segment with the signature residue at S_0) was selected because it indicates the direction of the helix immediately C-terminal to the signature residue. In addition, given that the S_1 residue is beyond the signature residue, the S_1 side chain does not influence the helical structure of the segment. The S_{-7}-S_{-6} segment was selected because it is the N-terminal segment closest to the noncanonical region that still has an α-helical structure. With few exceptions, these segments are suitable indicators of the change in helical direction across all classes of noncanonical structure: wide turns, tight turns, and kinks.

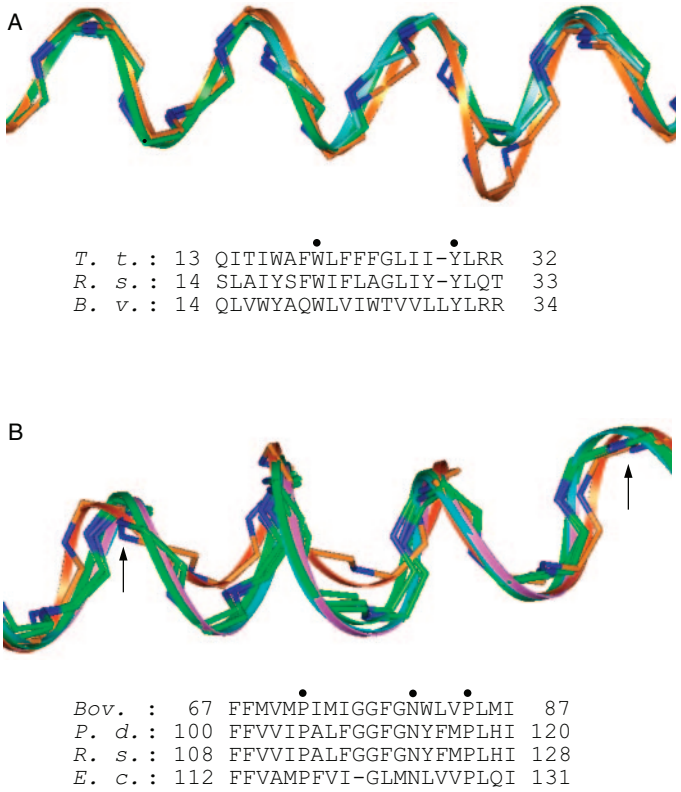

Fig. 2. Effect of an insertion or loss of a residue on the helical architecture of various transmembrane segments. A, insertion of a residue in an α-helical region is associated with a wide-turn noncanonical structure. This is shown with the transmembrane region of the H chain of *B. viridis* (*B. v.*). Alignment of this region with the corresponding transmembrane regions (both α-helices) of *R. sphaeroides* (*R.s.*) and *T. tepidum* (*T.t.*) shows the region containing Leu30 of *B. viridis* looping out as a widened turn (orange ribbon) before resuming as an α-helical structure. B, loss of a residue within a wide turn is associated with an α-helical structure. This is illustrated in the case of helix 2 in *Escherichia coli* ubiquinol oxidase (*E.c.*), which is homologous to the A chain of bovine (*Bov.*) cytochrome *c* oxidase (BCCO). In helix 2 in BCCO, there are conserved prolines at two positions (Pro72 and Pro84) and a conserved asparagine (Asn80). Aligning the ubiquinol oxidase with the *Paracoccus dentrificans* (*P.d.*) or *R. sphaeroides* (*R.s.*) BCCOs places the proline (Pro72) and asparagine (Asn80) residues (both inducing wide turns in the bovine) at comparable positions, with the N-terminal regions of the proline-induced wide turns all following a similar backbone path. However, the region between Pro117 and Asn124 of ubiquinol oxidase (equivalent to Pro72 and Asn80, respectively, of BCCO) is α-helical (orange ribbon), lacking the second wide turn as seen in the other three structures. Key conserved residues are indicated by dots. Arrows indicate positions of the two conserved prolines.

To assess the potential for backbone H-bond formation, the orientation of the C=O bond with respect to the helical axis was determined. For each segment in a wide turn region, the angle between the C=O bond and the helical axis was calculated. A backbone H-bond could form if the distance between the amide hydrogen atom donor and the carbonyl oxygen atom acceptor was $\leq$3.0Å and the C-H···O and H···O=C angles were $\geq$110° and $\geq$90° (Desiraju and Steiner, 1999), respectively.

Detailed Characterization of Wide Turns. With a regular α-helix, the Cβ atom of the side chain is directed toward the N terminus. To examine how and where the effects of the pyrrolidine ring of proline or the side chain of other signature residues start to affect helical structure in a noncanonical region, we chose to examine regions of the transmembrane helix extending from three positions C-terminal to eight positions N-terminal of the signature residue. This length of helix completely spans all noncanonical segments and, in addition, allows the steric effects of the pyrrolidine ring or other side chains that influence residues N-terminal to a noncanonical element to be characterized. Including residues beyond either end of wide-turn regions enabled parameters arising from coordinates spanning three or four residues; for example, inter-residue dihedral angles to be shown for the entire noncanonical region. Plots of the different parameters of these extended segments, therefore, include for comparison the capping helical structures at both ends of the perturbed region; such plots reveal whether an α-helical segment or another noncanonical segment is part of a region being investigated.

To orient noncanonical regions for comparison of structural features, the helical axis point for the signature residue at position *i* was placed at coordinates 0,0,0, and then the helical axis vector was rotated to lie along the positive *x*-axis (Supplemental Fig. 3). Having fixed the orientation of the helical axis vector (defined by the helical axis points for residues *i* and *i* + *1*), the entire helical region was then rotated to allow the $C\alpha_i$ atom to lie on the *z*-axis (that is, at coordinate 0,0,*z*, where *z* is equal to the radius of the segment from *i* to *i* + *1*); this orientation was designated the standard orientation.

Results and Discussion

More than 3000 individual transmembrane helical regions from 244 crystal structures deposited in the Protein Data Base (Berman et al., 2000) through August 2007 were examined. The dataset was restricted to crystal structures with resolution $\leq$3.0 Å and an *R* value $\leq$0.3. This set comprised 31 different proteins, including multichain protein complexes, with 350 transmembrane helices containing 70 wide turns. Although there is some uncertainty in the atom positions of structures with a resolution $>$ 2.2 Å but $<$ 3.0 Å, we included such structures, because, as noted by Senes et al. (2001), extended helical structures have an inbuilt degree of self-correction because the backbone atom positions have a greater degree of accuracy. NMR structures were considered, but were not included, with the exception detailed below, because the structures determined do not necessarily represent the lowest energy state of all segments of transmembrane helices. As a result, deviations in C=O and N-H bond orientations may limit the formation of potential backbone H-bonds.

Identification and Classification of Wide Turn Subclasses. Wide turns are characterized by the widening of a turn of a helix N-terminal to the signature residue or by the unwinding and lateral displacement of a two- to three-residue section of a helix (Fig. 1). As a result, the widened helix

contains ~4.4 residues per turn compared with 3.6 for an α-helix. This is evident, for example, in the H chain of the photosynthetic reaction centers of *Rhodobacter sphaeroides* and *Thermophilus tepidum*, each with a single α-helical transmembrane-spanning region. Alignment of these regions with the analogous region in the evolutionarily related organism, *Blastochloris viridis*, reveals the insertion of a single leucine residue (Leu30) in this transmembrane region, which, in contrast to the *R. sphaeroides* and *T. tepidum* structures, is a helix that now contains a wide turn (Fig. 2A). The opposite may also be the case (that is, deletion of a residue in an evolutionarily conserved transmembrane segment results in the switch from a wide turn to an α-helix) (Fig. 2B).

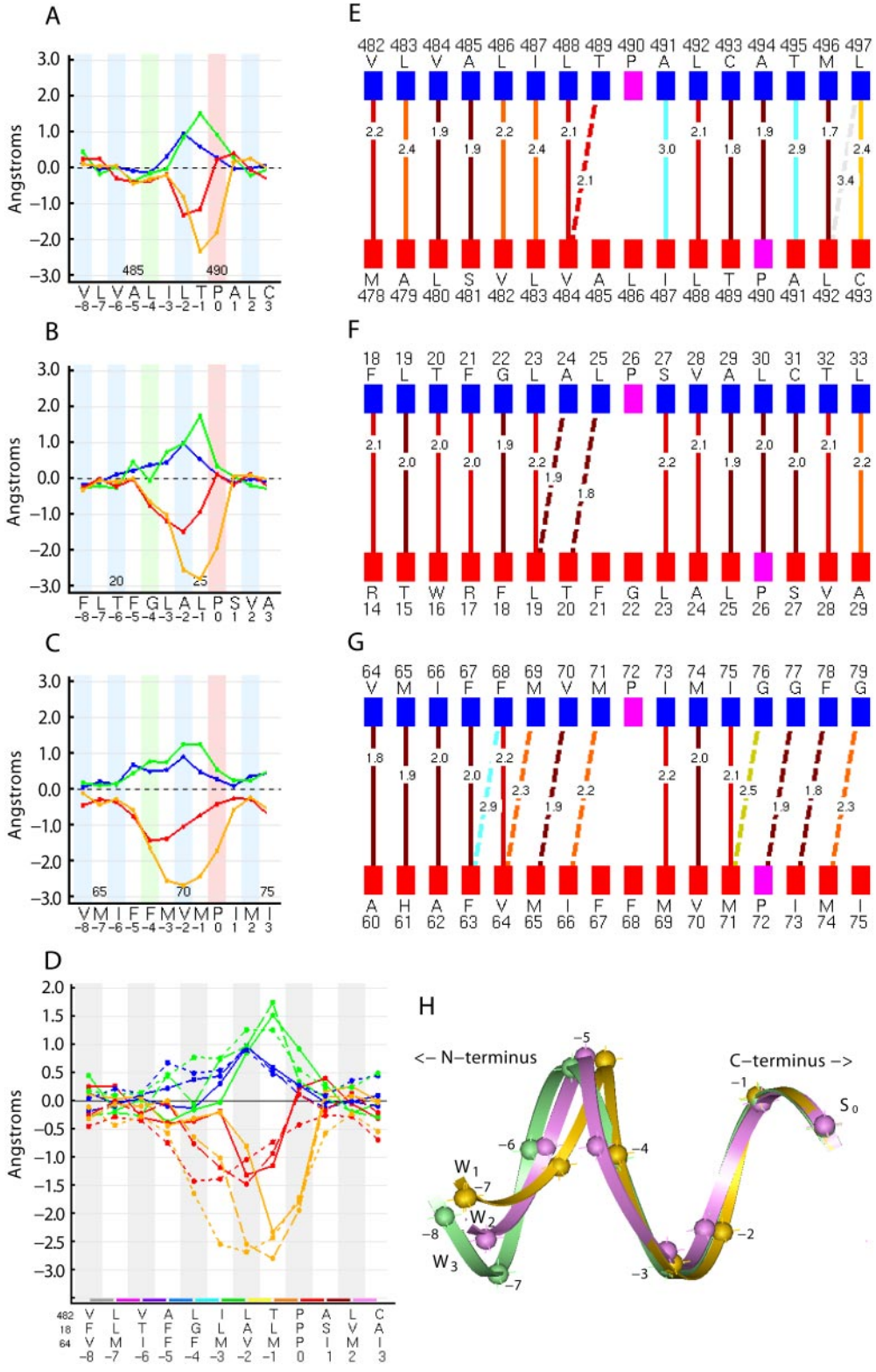

Fig. 3. $C\alpha_i \rightarrow C\alpha_x$ distance-difference profiles and H-bonding patterns for W_1, W_2, and W_3 wide turns. A–C, $C\alpha_i \rightarrow C\alpha_x$ distance-difference plots. Color code, difference between the distance between the Cα atom of any residue, n, in the noncanonical regions indicated and that of residues at 2 ($n-2$), 3 ($n-3$), 4 ($n-4$), 5 ($n-5$) positions N-terminal, and the comparable distances in an α-helix, are indicated by the blue, green, red, and yellow traces, respectively. A, W_1, *E. coli* Acrb multidrug efflux pump, helix 6, signature residue: Pro490. B, W_2, BCCO, G chain, helix 1, signature residue: Pro26. C, W_3, BCCO, A chain, helix 2: signature residue: Pro72. D, plots in A–C combined to allow comparison of differences in profiles. W_1 wide turn (——); W_2 wide turn (– –); W_3 wide turn (- - -). The colors of the flat rectangles on the *x-axis* correspond to the colors of the helical axis vector for each segment (see Fig. 5). E–G, H-bonding interactions in the proteins indicated in A–C, respectively, determined as described in Riek et al. (2001). Blue rectangles represent the amide hydrogen of the residue indicated, red rectangles represent the carbonyl oxygen, and pink rectangles denote prolyl residues. The amino acid sequences are indicated in the single letter code and are offset (from top to bottom) by four residues in keeping with the formation of n to $n-4$ H-bonds in an α-helix. Numbers above and below indicate sequence numbers. H-bond type: solid line (vertical): $i \rightarrow i-4$; dashed line (sloping from upper right to lower left): $i \rightarrow i-5$. Bond length (indicated by the numbers on the connecting lines) color code: brown, <2.0 Å; red, <2.2 Å; orange, <2.4 Å; orange-yellow, <2.5 Å; mustard yellow, <2.6 Å; green, < 2.7 Å; blue, < 2.8 Å; cyan, < 3.0 Å. H, different helical paths of the above W_1, W_2, and W_3 wide turns. The segments have been aligned such that the signature residues at position S_0 are coincident.

TABLE 1

Wide turn helical conformations in transmembrane proteins

Sequences containing the wide turn region are listed with the signature residue indicated in bold. The protein chain designation followed by the transmembrane helix number and the signature residue (SR) position and amino acid type are indicated. The PDB accession number identifies the crystal structure of the protein containing the wide turn.

Sequence	Chain	SR	PDB Code
W_1 subclass			
Proline			
VLVALILT**P**ALC	A6	490P	2J8S
YAIIYTIL**P**KQA	A6	252P	1XME
VVWAREYI**P**KIM	A11	473P	2A65
HAVHTYVK**P**FGD	A2	45P	2NWL
Nonproline			
LDVSAKVG**F**GLI	A7	219F	1C3W
LDVFAKYV**F**AFI	A7	245F	1E12
LDLVTKVG**F**GFI	A7	208F	1H2S
LPFFSKVG**F**SFL	A7	213F	1XIO
LDVTAKVG**F**GFV	A7	224F	1VGO
VYYLVGPM**T**ESA	A5	146T	1H2S
LWGIWNPL**R**AKT	A5	151R	1XIO
LYYLLTSL**R**SAA	A5	162R	1VGO
LSALVTDW**A**ASA	A5	184A	1E12
FLGFHSFG**L**YVH	A7	458L	1JB0
YLFTAIVG**A**MGW	B5	149A	1YEW
QKMAMFAG**G**ASG	C3	95G	1Q16
LLWWWYLG**G**AVE	A2	163G	2IC8
LSWFFIFG**G**MIE	A2	78G	2NR9
GLWGVTML**K**RLL	A9	303K	2NS1
AYVMAEQG**V**HVV	A7	222V	2NWL
W_2 subclass			
Proline			
FLTFGLAL**P**SVA	G1	26P	2DYR
LWLTFVYA**P**FAH	A4	131P	1U7G
VWLTLSYI**P**IAH	A4	142P	2B2H
FCVLQVFR**P**LLL	L3	136P	1VRN
YLTLVLFR**P**VMM	L3	136P	1AIJ
VLCIGCIH**P**TLV	M3	163P	1VRN
WMVLGFIR**P**ILM	M3	165P	1AIJ
GLGNFLRF**P**VQA	A1	32P	2A65
IAFLLVGI**P**LMW	A2	57P	2A65
YYVMRYIT**P**AFL	A11	457P	2A65
NMFFFDIY**P**YIA	C1	13P	1Q16
LEAVLFLL**P**WSF	A5	210P	1XME
FAYFLIIV**P**VIS	C8	368P	1KB9
FLLILVLM**P**TAG	C8	367P	1PPJ
GHQIHVSL**P**INK	A3	222P	1JB0
GHLIHVAI**P**ESZ	B3	199P	1JB0
IPVVCWLM**P**TVV	I1	23P	1JB0
YSAHTFVL**P**WLI	A6	192P	1VF5
LFIFVIVR**P**PIE	A3	75P	2HYD
Nonproline			
FYKFAVAE**K**RKK	I1	42K	2DYR
HFHYVLSM**G**AVF	A10	384G	2EIJ
FMVFGGFT**T**TLY	A2	93T	1U19
LWELVIEQ**F**EDL	A1	57F	1SU4
LFMTIPGI**A**LFY	A1	29A	1U7G
YVLFFGFT**S**KAE	A5	158S	1QKO
GGISKGIE**R**FAK	A5	193R	2A65
LWVNLVTD**G**LPA	A7	801G	2AGV
LYVIGVSC**T**YDV	A7	235T	2CFQ
AGGTVVHI**N**AAI	A5	170N	2NS1
LQILLVYF**V**LLK	A8	249V	2NWL
W_3 subclass			
Proline			
VMIFFMVM**P**IMI	A2	72P	2DYR
LMMFFVVI**P**ALF	A2	105P	1AR1
LMMFFVVI**P**ALF	A2	113P	2GSM
MFVVHFII**P**LIV	A5	215P	1U19
IIEFYLSY**P**IYI	C4	182P	1YEW
PFFIFIFG**P**LLQ	A3	97P	2CFQ
Nonproline			
PIMIGGFG**N**WLV	A2	80N	2DYR
PALFGGFG**N**YFM	A2	113N	1AR1
PALFGGFG**N**YFM	A2	121N	2GSM
YVLSMGAV**F**AIM	A10	387F	2DYR
YVMSLGAV**F**GIF	A10	422F	1AR1
NVIIGGVV**F**GCF	A10	430F	2GSM
HLAGLLGL**G**SLA	A3	208G	1JB0
HLAGLFGV**S**SLA	B3	185S	1JB0
GVLNAIVF**T**QLF	A2	81T	1XME
HLQVASLV**T**LTA	A10	394T	1XME
KAEVILGG**S**ISI	A7	296S	2A65
DFWAGTIG**V**VFF	A10	412V	2A65
TVVLLYLR**R**EDR	H1	34R	1VRN
YLVCFCFF**K**QLA	A11	358K	2CFQ

To define wide-turn regions in transmembrane segments, we used $C\alpha_i \rightarrow C\alpha_x$ distance-difference profiles, because they are distinctive for such noncanonical structures and can readily discriminate between these and other noncanonical elements (tight turns or kinks) (Supplemental Fig. 1). However, it was evident from such profiles that the width of the $C\alpha_{i-4}$ and $C\alpha_{i-5}$ traces varied (Fig. 3) and that these variations were directly related to the number of potential π H-bonds that could be formed N-terminal to the signature residue, S. Thus, although differences in the width of the $C\alpha_{i-4}$ and $C\alpha_{i-5}$ traces identified potential subclasses of wide turns, because the difference in the number of potential π H-bonds formed is a discrete variable, this was used as the basis for subclassifying them into three distinct subclasses as follows: W_1, one π H-bond between S_{-1} and S_{-6} (Fig. 3, A and E); W_2, two π H-bonds between S_{-1} and S_{-6}, and S_{-2} and S_{-7} (Fig. 3, B and F); and W_3, three or more π H-bonds including those between residues at positions S_{-1} and S_{-6}, S_{-2} and S_{-7}, and S_{-3} and S_{-8} (Fig. 3, C and G), (Table 1). The additional π H-bonds formed with the W_2 and W_3 wide turns involve interactions with residues N-terminal to the signature residue (Fig. 3D). Non–proline-induced wide turns have the potential to form an additional π H-bond between the amide hydrogen atom of the signature residue and the carbonyl oxygen atom of the residue at position S_{-5}. In such cases, the subclassification continues to be that based on the number of π H-bonds formed from the S_{-1} position. The distribution of proline- and non–proline-induced wide turns of each class is shown in Table 2.

As shown in Table 3, the range of ϕ and ψ values at the S_{-5} to S_{-3} positions for the different wide-turn subclasses overlap and cannot be used to distinguish among them. Likewise, as noted by Fodje and Al-Karadaghi (2002; see Figure 2a therein), although a number of points lie outside the "preferred" region in the Ramachandran ϕ-ψ plot (Lovell et al., 2003) for the residues at the π5 position, (equivalent to the S_{-3} position in our study), a comparable number lie within the "preferred" region. Indeed, analysis of the ϕ/ψ dihedral angles lead us to use the term "wide turn" instead of "π-bulge," given that if the individual pairs of averaged ϕ and ψ dihedral angles determined for the S_{-5} to S_{-2} positions (Table 3) are used to construct regular helices, none form a π-helix (that is, a helix with 4.4 residues per turn and $i \rightarrow i-5$ H-bonding). In fact, the different ϕ and ψ combinations

TABLE 2

Distribution of proline- and non–proline-induced wide turn subclasses

	W_1	W_2	W_3	$W_1 + W_2 + W_3$
Proline	4 (6%)	19 (27%)	6 (8%)	29 (41%)
Nonproline	16 (23%)	11 (16%)	14 (20%)	41 (59%)
Total	20 (29%)	30 (43%)	20 (28%)	70

for the S_{-3} position all produce either a left-handed helix or a circular helical path with a rise per residue of ~0 Å—a structural impossibility. Likewise, the ϕ and ψ values for position $\pi 5$ (S_{-3}) (Table 3 of Fodje and Al-Karadaghi, 2002) also produce a circular structure. Most of these structures cannot form because of severe steric clashes between atoms on the adjacent turns. In addition, no ϕ and ψ angle combinations yield a helix with π H-bonding as the major H-bond type. Although a π-bulge appears to mimic a segment of π-helix, the backbone dihedral angles indicate that it forms a structure with less than perfect π-helical character. Thus, ϕ and ψ dihedral angles, per se, can be used neither to characterize wide turns nor to discriminate between different noncanonical types.

In several instances of wide turns, the number of π H-bonds indicated by H-bonding diagrams is fewer than the number expected based on the subclass indicated by the $C\alpha_i \rightarrow C\alpha_x$ distance-difference profile. One such example is the wide turn induced by Pro215 in helix 5 of bovine rhodopsin (Protein Data Base code 1U19). This has a $C\alpha_i \rightarrow C\alpha_x$ distance-difference profile typical of the W_3 subclass (Fig. 4A), but the H-bonding diagram indicates only two rather than three π H-bonds (Fig. 4B). This is due to the combination of a ψ angle at position 211 that is less negative (53° versus −40°) than for an α-helix and a ϕ angle that is more negative (−180° versus −65°) at position 212. This forces the His211 C=O bond to deviate from its normal direction by 75° (Fig. 4C). This marked deviation of the 211 C=O bond is associated with a coincident reorientation of the H-N bond at position 212, which positions its hydrogen atom below the 110° cutoff angle (H-N···O) required for the formation of an $S_{-3} \rightarrow S_{-8}$ π H-bond. It is clear from a consideration of such aberrant wide turns that they could well be missed if their identification was based merely on the number of π H-bonds. In contrast, our method of detecting wide turns based on Cα positions, which are the least likely to be perturbed even with wide turns that show the most marked structural deviation from that of an α-helix, is much more robust.

In addition to the aberrant wide turn examples considered above that show very marked deviations in the C=O bond away from the helical axis, as noted by Fodje and Al-Karadaghi (2002) and Cartailler and Leucke (2004), almost all wide

TABLE 3

ϕ and ψ dihedral angles ± 1 S.D. for the different subclasses of wide turns

0 marks the position of the signature residue. Negative values indicate positions N-terminal to the signature residue. Position 3 in the helix-C region in the results of Cartaillier and Luecke (2004) is equivalent to the position of the signature residue. In the Fodje and Al-Karadaghi study (2002), position + 1 corresponds to the signature residue position.

RP	W_1		W_2		W_3		$W_1 + W_2 + W_3$	
	ϕ	ψ	ϕ	ψ	ϕ	ψ	ϕ	ψ
Proline-induced								
−8	−68 ± 7	−36 ± 10	−68 ± 21	−49 ± 24	−53 ± 12	−48 ± 6	−65 ± 19	−47 ± 20
−7	−64 ± 6	−44 ± 8	−66 ± 6	−38 ± 8	−66 ± 11	−50 ± 9	−65 ± 7	−41 ± 10
−6	−65 ± 2	−43 ± 4	−62 ± 6	−48 ± 7	−72 ± 7	−43 ± 16	−64 ± 7	−46 ± 9
−5	−68 ± 3	−27 ± 11	−76 ± 18	−38 ± 7	−90 ± 23	−40 ± 12	−78 ± 19	−37 ± 10
−4	−91 ± 10	−30 ± 16	−92 ± 11	−22 ± 12	−107 ± 9	6 ± 15	−95 ± 12	−17 ± 18
−3	−114 ± 10	−20 ± 26	−121 ± 16	−54 ± 10	−132 ± 16	−62 ± 9	−122 ± 16	−51 ± 18
−2	−113 ± 25	−45 ± 4	−64 ± 12	−55 ± 7	−66 ± 6	−56 ± 8	−71 ± 22	−54 ± 8
−1	−59 ± 7	−39 ± 8	−58 ± 7	−49 ± 5	−58 ± 8	−50 ± 4	−58 ± 7	−48 ± 6
0	−57 ± 3	−37 ± 6	−59 ± 6	−41 ± 9	−55 ± 4	−47 ± 9	−58 ± 5	−42 ± 9
1	−68 ± 6	−38 ± 5	−67 ± 9	−39 ± 10	−59 ± 13	−49 ± 10	−65 ± 10	−41 ± 10
2	−71 ± 6	−29 ± 9	−57 ± 34	−41 ± 9	−69 ± 15	−53 ± 14	−62 ± 29	−42 ± 13
3	−79 ± 11	−36 ± 11	−62 ± 24	−31 ± 18	−69 ± 14	−48 ± 9	−66 ± 22	−35 ± 17
Non–proline-induced								
−8	−60 ± 4	−44 ± 5	−66 ± 8[a]	−41 ± 13[a]	−65 ± 7	−42 ± 9	−63 ± 7	−42 ± 12
−7	−59 ± 5	−45 ± 7	−65 ± 6[a]	−39 ± 8[a]	−69 ± 8	−4 ± 414	−60 ± 29	−41 ± 17
−6	−62 ± 5	−44 ± 4	−65 ± 6	−35 ± 26	−79 ± 14	−52 ± 8	−68 ± 12	−44 ± 16
−5	−66 ± 6	−42 ± 12	−87 ± 23	−44 ± 14	−82 ± 6	−48 ± 18	−78 ± 16	−45 ± 15
−4	−73 ± 15	−21 ± 18	−79 ± 18	−32 ± 22[b]	−80 ± 20	−27 ± 19	−79 ± 18	−22 ± 27
−3	−106 ± 21	−70 ± 14	−103 ± 26	−56 ± 20	−99 ± 18	−69 ± 13	−104 ± 20	−64 ± 20
−2	−69 ± 16	−44 ± 10	−62 ± 28	−53 ± 21	−60 ± 8	−47 ± 9	−65 ± 16	−49 ± 12
−1	−63 ± 5	−43 ± 7	−53 ± 23	−36 ± 15	−63 ± 6	−41 ± 11	−62 ± 9	−41 ± 10
0	−62 ± 7	−39 ± 22	−62 ± 8	−46 ± 7	−69 ± 10	−37 ± 11	−64 ± 9	−40 ± 16
1	−67 ± 24	−39 ± 10	−66 ± 7	−40 ± 6	−69 ± 10	−43 ± 13	−68 ± 16	−41 ± 11
2	−64 ± 5	−36 ± 29	−62 ± 6	−43 ± 9	−69 ± 11	−41 ± 11	−65 ± 8	−40 ± 20
3	−67 ± 19	−39 ± 8	−65 ± 8	−39 ± 10	−65 ± 13	−36 ± 20	−66 ± 15	−37 ± 14
Combined proline- and non–proline-induced								
−8	−61 ± 6	−43 ± 7	−67 ± 17	−45 ± 23	−62 ± 10	−44 ± 9	−64 ± 13	−44 ± 16
−7	−60 ± 5	−45 ± 7	−59 ± 34	−36 ± 17	−68 ± 9	−46 ± 13	−62 ± 23	−41 ± 15
−6	−62 ± 4	−44 ± 4	−63 ± 6	−43 ± 18	−76 ± 13	−49 ± 12	−67 ± 10	−45 ± 14
−5	−67 ± 6	−39 ± 13	−81 ± 20	−40 ± 11	−84 ± 14	−46 ± 17	−78 ± 17	−41 ± 14
−4	−77 ± 16	−23 ± 18	−90 ± 15	−20 ± 28	−88 ± 21	−17 ± 23	−85 ± 18	−20 ± 24
−3	−108 ± 20	−60 ± 26	−116 ± 18	−53 ± 18	−109 ± 23	−67 ± 13	−112 ± 20	−59 ± 20
−2	−78 ± 25	−44 ± 9	−64 ± 17	−57 ± 10	−62 ± 8	−50 ± 10	−67 ± 19	−51 ± 11
−1	−62 ± 6	−42 ± 7	−58 ± 11	−45 ± 9	−62 ± 7	−43 ± 11	−60 ± 9	−44 ± 9
0	−61 ± 7	−38 ± 20	−60 ± 7	−43 ± 9	−65 ± 11	−40 ± 11	−61 ± 8	−41 ± 14
1	−67 ± 21	−39 ± 10	−67 ± 8	−39 ± 8	−66 ± 12	−45 ± 12	−67 ± 14	−41 ± 10
2	−65 ± 6	−35 ± 27	−59 ± 28	−42 ± 9	−69 ± 12	−45 ± 13	−64 ± 20	−41 ± 17
3	−70 ± 19	−38 ± 9	−63 ± 20	−33 ± 16	−66 ± 13	−39 ± 18	−66 ± 18	−36 ± 15

RP, residue position.

[a] One point removed from each set because the positions were beyond the helical region (helix A5, 2NS1).

[b] One value removed because a *cis* peptide bond 25I-26P produces 25I ψ angle of + 100° skews the results if included.

turns result in some degree of C=O bond deviation and, therefore, might be unable to form hydrogen bonds with amide hydrogen atoms in the adjacent C-terminal turn. With few exceptions, all proline-induced wide turns cause a deflection of the S_{-4} (and in some instances the S_{-5}) C=O peptide bond by more (up to an additional 60°) than the ~18° observed in an α-helix. This prevents a steric clash with the Cδ methylene moiety of the pyrrolidine ring and allows the amide hydrogen atoms of the residues on either side of proline to be located within H-bonding distance of the carbonyl oxygen atoms on the widened turn. The more negative the dihedral angles of the residue at position S_{-3} and the greater the difference between the S_{-3} ϕ and S_{-4} ψ dihedral angles, the greater the deviation of the peptide bond plane with respect to the helical axis. However, the larger deviations do not always prevent a π H-bond from forming.

Influence of Wide-Turn Subclasses on Helical Architecture. Residues in the vicinity of wide-turn signature residues can also have a modifying effect on helical structure. To evaluate such effects, we examined noncanonical regions on a residue-to-residue basis. To this end, we determined the changes in direction of the helical axis vector at each position (Fig. 5) and examined the effects on the different wide turns arising from sequence and rotamer differences. By compar-

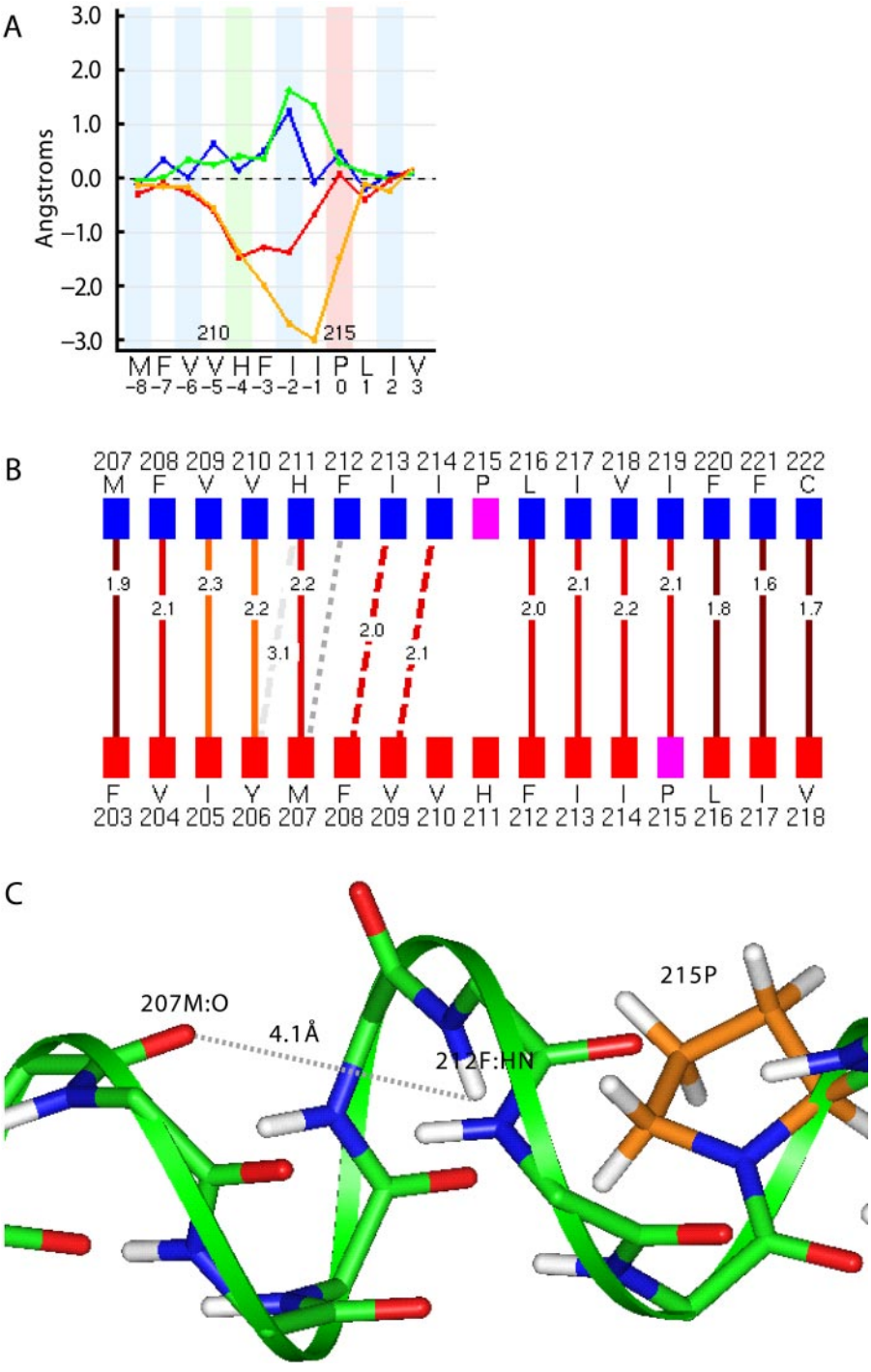

Fig. 4. A W_3 wide turn with fewer than predicted π H-bonds. A, the $C\alpha_i \rightarrow C\alpha_x$ distance-difference plot of a noncanonical region spanning Met207 to Leu216 in helix 5 of bovine rhodopsin indicates a W_3 wide turn based on the width of the negative deflections (red and yellow traces). B, H-bonding diagram indicating that the π H-bond between Met207:O and Phe212:HN does not form. The absent π H-bond between Met207:O and Phe212:HN is indicated by the gray dotted line. C, helical structure of the noncanonical region containing the wide turn induced by Pro215 shows the skewed orientation of the His211 C=O bond as a result of its ψ dihedral angle being markedly less negative (+53°) than that of an α-helix (−40°). This also produces a coincident reorientation of the H-N bond at position 212, leading to the distance between Met207:O and Phe212:HN (4.1Å) being too great to allow an H-bond to form. In addition, the orientation of the Phe212 HN bond, directed toward the helical axis, results in an *N*-H···O angle of 60°—much less than the minimum 110° required for an H-bond.

ing the differences in direction (helical bend angle) and position between the reference axis vector and the vector for the S_{-7}-S_{-6} segment (the last α-helical segment before the beginning of a noncanonical region), it is possible to measure the different wide turns (Fig. 5). When the helical axis vectors determined between adjacent N, Cα, or C groups of atoms of the peptide backbone are displayed concurrently, the effect of each backbone dihedral angle on helical structure and direction is revealed (Fig. 5, A, E, and F).

Analysis of the helical bend angles shows differences between wide-turn subclasses but also within subclasses. Except for the W_3 subclass, proline-induced wide turns show greater bend angles, and a narrower range of bend angles, than do the wide turns induced by nonproline amino acids (Table 4). With the diversity of side-chain structure for the nonproline amino acids, the wider range in bend angles is not unexpected. Although the signature residue, particularly if proline, is the major disruptive influence on the integrity of α-helical structure, residues within the wide-turn region also have an effect on the direction of the helix. This is seen with the shifts in position and direction of the axis vectors for the intermediate segments compared with the reference segment vector (Fig. 5, E and F). These shifts indicate that the change in helical direction is not limited to a single point on the helix but is the result of cumulative changes occurring over a number of segments. Figure 5, A–C, shows the paths of the N-terminal helical segments of a proline-induced wide turn of each subclass and the extent of the shift in helical axis. It is evident from Fig. 5 that the W_1 subclass produces the largest shift in the helical axis in the region immediately N-terminal to the helical perturbation. The path traced by the axis vectors shows that for proline-induced wide turns, the backbone loops around the pyrrolidine ring and then bends away from the proline.

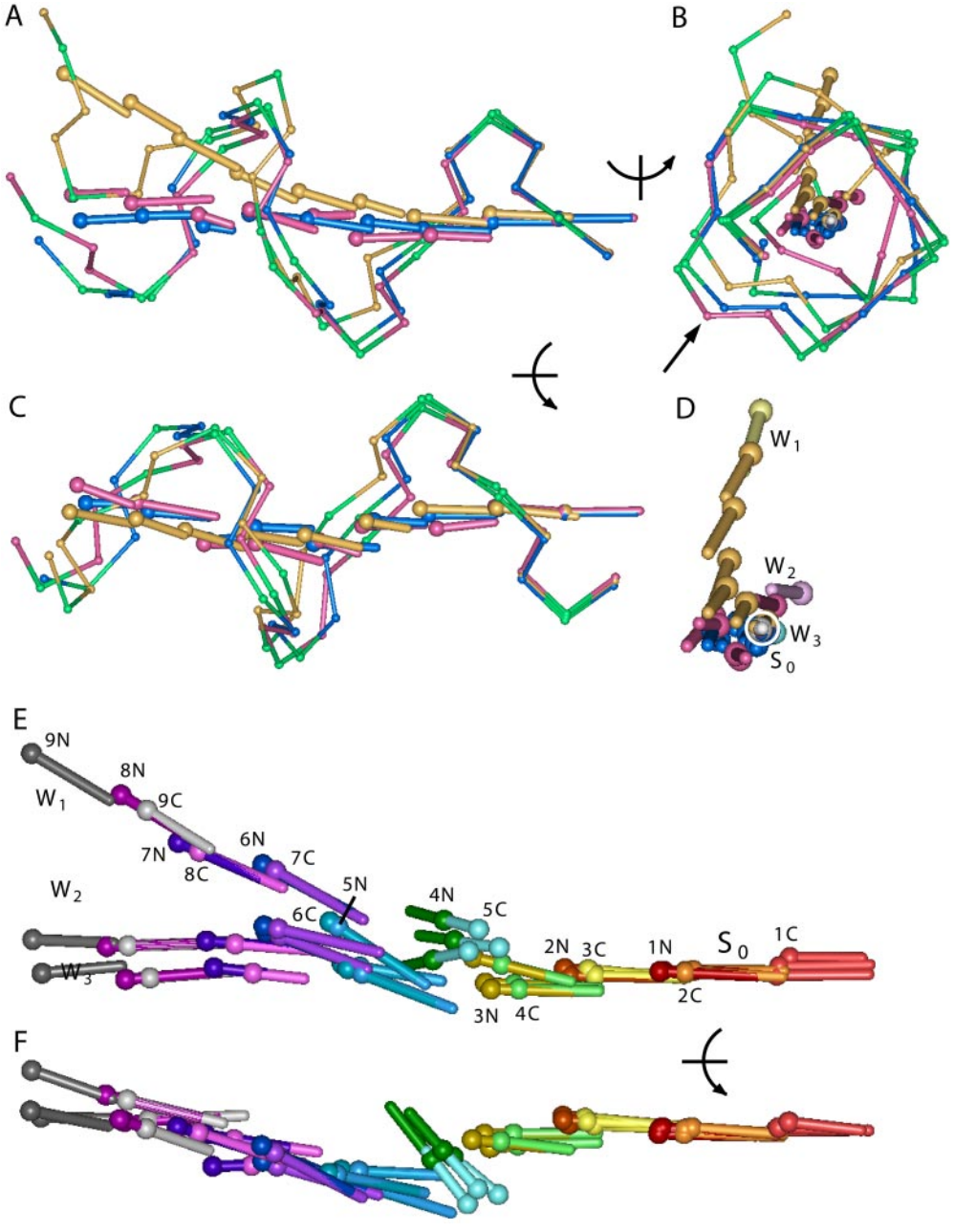

Fig. 5. Position and direction of $N_i \rightarrow N_{i+1}$, $C\alpha_i \rightarrow C\alpha_{i+1}$, and $C_i \rightarrow C_{i+1}$ helical axis vectors over the noncanonical region for proline-induced W_1 (yellow), W_2 (pink), and W_3 (blue) wide turns. (Note: the axis vectors of an α-helix would form a straight line.) An example from each wide turn subclass was placed in the "standard" orientation and combined to form a single display. The $C\alpha_{S0} \rightarrow C\alpha_{S+1}$ reference segment vector and the preceding eight N-terminal $C\alpha_i \rightarrow C\alpha_{i+1}$ vectors are shown along with the backbone N, Cα, and C atoms. Examples: W_1 subclass induced by Pro490 in helix 6 of *E. coli* Acrb multidrug efflux pump (yellow); W_2 subclass induced by Pro26 in helix 1 of the G chain of BCCO (pink); W_3 subclass induced by Pro72 in helix 2 of the A chain of BCCO (blue). A, view along the *z*-axis. B, view along the *x*-axis. C, view along the *y*-axis. The N, Cα, and C backbone atoms indicate the path of the helix and show the backbone at the S_{-4} position looping out around the position (arrow) of the pyrrolidine ring (not shown). D, a view similar to B, with the backbone atoms removed and the S_0 position highlighted by a white circle. The extent of the change in the vectors is indicated by the lighter coloring of the S_{-8} vectors. The W_1 wide turn shows the greatest change in helical direction, the W_2 wide turn a smaller divergence, and the W_3 minimal change in direction. E and F, helical axis vectors of the same noncanonical segments as in A–D but determined based on the N and C atoms. The orientations are the same as shown in A and C, above, with the N and C vectors in E labeled showing position N-terminal to S_0. The orientations of the $N_i \rightarrow N_{i+1}$ and $C_i \rightarrow C_{i+1}$ axis vectors are similar to the $C\alpha_i \rightarrow C\alpha_{i+1}$ vectors with the exception of the $C_{S-4} \rightarrow C_{S-3}$ and $N_{S-3} \rightarrow N_{S-2}$ axis vectors, which show a reversed direction and indicate segments with a left-handed orientation. Color code: S_0 or reference vector, light (C series) and dark red (N series); S_{-1}, orange; S_{-2}, yellow; S_{-3}, green; S_{-4}, cyan; S_{-5}, blue; S_{-6}, purple; S_{-7}, dark pink; S_{-8}, gray.

With proline-induced wide turns, the pyrrolidine ring and the formation of a single π H-bond act as the equivalent of inserting a "wedge" into the helix, forcing it to bend away from the side containing the proline. With each additional π H-bond formed in the W_2 and W_3 wide turns, another wedge is inserted into the helix but at an orientation equivalent to the position of the additional π H-bond. The effect or "shape" of the wedge will be dependent upon the effects of the residues within the wide turn. Given that W_3 wide turns have three or more π H-bonds, the combined effect can offset the effect of each individual π H-bond, resulting in negligible change in helical direction.

Aromatic, β-branched, and large-volume residues predominate in the eight positions N-terminal to the signature residue in proline-induced wide turns, whereas glycine, alanine, serine, and threonine are usually found at two or more positions within this region in wide turns with a nonproline residue at the signature position. W_3 wide turns have a greater proportion of large volume residues compared with the W_1 and W_2 subclasses. Examples from a wider range of transmembrane protein families are needed before residue patterns characterizing each subgroup can be determined. Although wide turns are found throughout the transmembrane region, the majority of available examples lie toward the C-terminal region. However, there were a number of N-terminal region wide turns that were not included in the survey because they were either incomplete, in that they occurred in the last turn of the helix where the partial wide turn transitioned into coil-like or other nonhelical geometries before the wide turn was completed, or the remaining N-terminal portion of the helix was one turn or less in length.

Although structures solved by NMR do not provide consistent H-bonding patterns to allow confident delineation of wide-turn subclasses, the $C\alpha_i \rightarrow C\alpha_x$ distance-difference profiles can be used to study the structure of the helical transmembrane segments. Analysis of the NMR-derived structures of PufX (Tunnicliffe et al., 2006), a single transmembrane-spanning protein organizing the photosynthetic reaction center (RC)-light harvesting complex of *R. sphaeroides* revealed up to four regions displaying profiles with wide turn characteristics (Supplemental Fig. 4). Calculation of the mean and standard deviations of the $C\alpha_i \rightarrow C\alpha_x$ distance differences determined for these various NMR structures, at each position, revealed some segments that are relatively fixed and others where the helical architecture is flexible, varying between wide turn and almost α-helical geometries [e.g., the segment encompassing residues 34 to 37] (Fig. 6). In a number of purple bacteria, the photosynthetic RC is surrounded by a ring of light-harvesting $\alpha\beta$ polypeptide chains (LH1). The RC reduces a quinone (Q_B) successively over a number of cycles, and when fully reduced, it moves from the RC through the membrane to an adjacent cytochrome bc_1 complex (Cogdell et al., 2006). In *R. sphaeroides*, PufX is proposed to fulfill two functions: to enable the formation of a LH1-RC dimer and to provide a gap in the LH1 ring to allow the delivery of Q_B to the bc_1 complex. The glycine zipper motifs present in PufX would stabilize dimer formation. Thus, it seems reasonable to suppose that flexibility in the transmembrane region of PufX is required to provide an opening within the bilayer for Q_B to move within the membrane, while at the same time maintaining its contacts with the LH1-RC dimer complex.

TABLE 4
Helix bend angles

	W_1	W_1	W_3
Proline	40 ± 5°[a]	23 ± 7°	14 ± 6°
Non-proline	22 ± 7°	14 ± 9°	11 ± 7°

[a] Mean ± 1 S.D.

Rotamer Involvement in Proline and Nonproline Wide Turns. Proline, unlike other residues with side chains that can rotate around the Cα-Cβ bond, is restricted to a single rotamer conformation with limited flexibility provided only by ring isomerization between *exo* and *endo* forms. With nonproline residues, one or more rotamer conformations is found in both wide turns and α-helices (Dunbrack and Cohen, 1997; Lovell et al., 2000). This flexibility allows a wide turn to change its position along a transmembrane helical segment provided that the signature residue is not a proline.

An example of such a switch in the position of a wide turn is seen in helix 10, subunit I of bovine cytochrome *c* oxidase (BCCO) (Tsukihara et al., 2003; Muramoto et al., 2007). In the reduced state, the wide turn has a W_2 profile with Gly384 as the signature residue. In the oxidized form, however, a W_3 wide turn is present with the signature residue position now at Phe387 (Fig. 7). To allow this isomerization to a different signature residue, two residues within this region (Leu381 and Ser382) have had to change their rotamer conformations (Fig. 7). Moreover, the wide turn has introduced a region of flexibility that is not available with an α-helical geometry, or with a tight turn or kink.

Modifying Effects of Other Residues. The effects of residues apart from the signature residue on helical direction are demonstrated by the structures of helix 5 of bacterial rhodopsins. Two such structures have a proline at the S_{-2} position of W_1 non–proline-induced wide turns (Fig. 8A). These S_{-2} prolines not only alter the direction of the helix (Fig. 8A) but also cause its marked lateral displacement (Fig. 8, B and C) in the region N-terminal to the prolines, to allow the bulky pyrrolidine rings to be accommodated. This mechanism of pyrrolidine ring-accommodation differs from that used by other noncanonical helices in which there is little lateral displacement of the helix. Rather, the helix in the immediate N-terminal region loops out to accommodate the pyrrolidine ring (Fig. 1A, orange ribbon). Because the S_{-2} prolines prevent the wide turn from being propagated more N-terminally, only a single $S_{-1} \rightarrow S_{-6}$ π H-bond is formed.

Because glycyl residues lack a side chain, the preceding N-terminal portion of the helix can be oriented more closely to the glycine than it could for a residue with a side chain. In addition, the lack of a side chain allows a greater depolarization of the Cα-Hα1 and Cα-Hα2 bonds, allowing the Hα1 and Hα2 atoms to form stronger H-bonds, ~−2 kcal/mol (Vargas et al., 2000; Scheiner et al., 2001), relative to CH···O H-bonds formed by H atoms not bound to the backbone Cα atom [~−0.5 kcal/mol (Desiraju and Steiner, 1999)]. The Hα1 atom of glycine forms an intrahelical H-bond with the carbonyl oxygen of the *i−4th* residue on the preceding turn. Evaluation of 18 wide turns with a glycine at position S_{-1} shows that the S_{-5} position is closer to the S_{-1} position by 1.1 to 1.7 Å compared with wide turns with S_{-1} residues other than glycine (Supplemental Fig. 5). The presence of the glycine can change helical direction by ~5°.

Structural Effects of Wide-Turn Subclasses. Wide turns alter the register of a face of a helical segment C-terminal to the turn, compared with the orientation of the

face before the turn, and the extent of this shift differs between the subclasses. It is smallest for the W_1 subclass (~45°–75°), intermediate for the W_2 subclass (60°–90°) and largest for the W_3 subclass (80°–120°). This provides flexibility in helical architecture, allowing interactions between residues on the transmembrane segment in question with those on an adjacent helix, and in particular, allows backbone-to-backbone interactions that would otherwise not be possible with a rigid α-helical structure.

An example of two wide turns underlying such interhelical interactions is shown in Fig. 9. Here, a number of CH···O type H-bonds (predominantly CαH···O) stabilize interactions between transmembrane helix 1 of the A chain of BCCO, involving a glycine zipper motif (GxxxGxxG) (MacKenzie et al., 1997; Russ and Engelman, 2000; Senes et al., 2000, 2004; Kim et al., 2005), G_{23}AWAGMVG$_{30}$, and helix 2, which is in an antiparallel orientation to helix 1 and contains two wide turns. Both wide turns belong to the W_3 subclass and produce <5° changes in helical direction. As is evident, the first wide turn of helix 2 orients the C=O bond of residue Phe68 such that it interacts via a CH···O H-bond with the Hα2 atom of Gly23 in helix 1. Likewise, the second wide turn orients the C=O bond of Gly76 in helix 2 such that it can interact via a CH···O H-bond with Hα2 of Gly16 in helix 1. These interactions would not be possible if helix 2 lacked these wide turns, because the C=O bonds of Phe68 and Gly76 would not be directed toward their respective H-bonding partner residues. Moreover, the widening of the helix at the positions of the two wide turns brings these residues to within H-bonding distance of the adjacent helix. Note that because Phe68 and Gly76 bond to glycine donors (Gly23 and Gly16), the CαH···O bonds thus formed are stronger than usual CH···O bonds (Desiraju and Steiner, 1999; Vargas et al., 2000; Scheiner et al., 2001). The lack of side chains on these glycines also facilitates interhelical packing that sterically would not be possible if residues containing side chains occupied these positions (Fig. 9). Finally, because wide turns permit backbone-to-backbone interactions, the interacting helices pack more closely than would be possible with interactions involving side chain-to-backbone or side chain-to-side chain bonding, because the number of contacts, electrostatic or van der Waals, that can form with these latter interactions, is likely to be less. Other examples of a glycine zipper motif stabilizing interhelical contacts have been reported (Senes et al., 2000), but to our knowledge this is the first example of a glycine zipper interacting with a wide turn.

In contrast to these W_3-mediated interhelical interactions, interhelical interactions involving helices with W_1 and W_2 wide turns do not involve glycyl residues but rather residues that have side chains with conventional H-bond donor properties. Moreover, the larger helical bend angles of the W_1 and W_2 subclasses (Table 4) limit the contacts between adjacent helices to only one or two H-bonding interactions. Nonetheless, the stronger conventional N/O-H···O H-bond formed in these cases may be required, given the limitation to only one or two interhelical H-bond interactions. Typically, these H-bonds are backbone-to-side chain interactions usually involving tryptophan (Hε1 atom), serine (Hγ1), or threonine (Hγ1). The larger helical bends of the W_1 and W_2 wide turns and the involvement of a residue with a side chain for interaction, provide the flexibility required to allow the helix containing such turns, and an adjacent interacting helix, to be oriented in either a parallel or antiparallel fashion.

With the W_3 turns involving glycyl donors, although both the Hα1 and Hα2 atoms can form H-bonds, their H-bonding roles are distinct. The Hα1 atom is involved in intrahelical H-bonding or interhelical H-bonding to a carbonyl oxygen on an adjacent helix that runs in a parallel orientation. In contrast, the Hα2 atom can only form interhelical H-bonds with a backbone carbonyl on an adjacent helix if it runs in antiparallel orientation. This orientation is required; a parallel orientation precludes H-bonding because both the Cα-Hα2 bond and the C=O bond are aligned in the same direction.

Binding of Cofactors, Ions, and Ligands. Wide turns have previously been noted to provide binding site for cofactors and ions (Fodje and Al-Karadaghi, 2002; Cartailler and Luecke, 2004). Several interesting examples are also evident from our analyses. For example, a W_2 non–proline-induced wide turn is evident in helix 10 of the A chain of BCCO that binds the cofactor, HEME-A. A W_2 wide turn (signature residue Gly801) is also seen in the absence of Ca^{2+} in helix 7 of rabbit muscle Ca^{2+} ATPase. However, in the presence of Ca^{2+}, the wide turn structure is disrupted because residues previously involved in

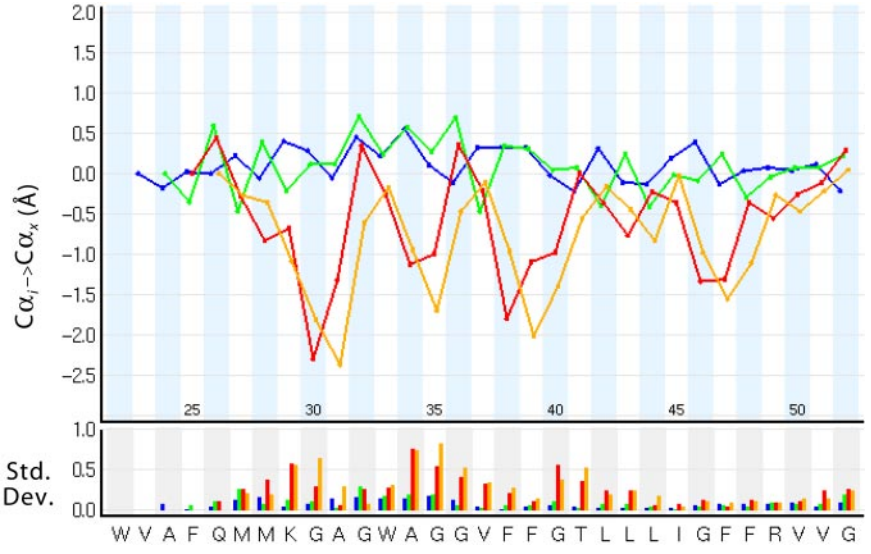

Fig. 6. Mean Cα_i→Cα_x distance-differences (top) and their standard deviations (histogram, bottom) for the helical region of PufX. The mean Cα_i→Cα_x distance-difference profiles show the presence of four regions with wide-turn characteristics at Gly30, Gly35, Gly40, and Phe47 in the transmembrane segment (Trp22 → Gly52). As is evident from the standard deviation histograms, the wide turn at Phe47 shows very little variation in Cα_i→Cα_x distance-differences compared with the other three wide turns. Consistency of the Phe47 wide-turn structure is probably the result of hydrophobic/aromatic interactions between Trp33 and Val37 and between Phe38 and Leu42. Color codes as indicated in Fig. 3.

forming it now use their carbonyls to form a Ca^{2+} binding pocket. Finally, a proline-induced W_2 wide turn in helix 5 of bovine rhodopsin helps to correctly position residues that line the binding pocket for the β-ionone ring of retinal. Upon photoactivation and isomerization of the chromophore from 11-*cis* to all-*trans* retinal to form the LUMI rhodopsin photo-intermediate, the β-ionone ring is now oriented so that it can interact with the S_{-4} carbonyl oxygen of the wide turn (Nakamichi and Okada, 2006).

With the recent release of the structure for another member of the G-protein-coupled superfamily, the β_2-adrenergic receptor (AR) (Cherezov et al., 2007), we can now identify regions within the transmembrane helices that differ from those of rhodopsin. Although the transmembrane domains (TM) in the two structures have similar orientations, there are both similarities and differences in their wide turns, the latter potentially being important for receptor activation by their distinctive ligands—biogenic amines in the case of the β_2-AR and 11-*cis* retinal in the case of rhodopsin. These include a wide turn in TM II of both receptors that in both instances is of the W_2 subtype, and one in TM V that is of the W_3 subtype in rhodopsin but is a W_2 wide turn in the β_2-AR. The β_2-AR also has a W_1 wide turn induced by Pro168 in TM IV, with the carbonyl bond of Thr164 at the S_{-4} position of this wide turn being directed toward Ser203 on TM V. Although Thr164 and Ser203 are too widely separated to form an H-bond, it is of interest that Ser203 is critically involved in ligand binding, via an H-bond interaction with the *m*-hydroxyl of the catechol ring, as well as in receptor activation (Strader et al., 1989; Liapakis et al., 2000). Thus, Thr164 in the β_2-AR may be important for positioning the ligand to allow interaction between Ser203 and its *m*-hydroxyl. Rhodopsin has a proline-induced kink rather than a wide turn at the equivalent region in TM IV that, in contrast to the β_2-AR,

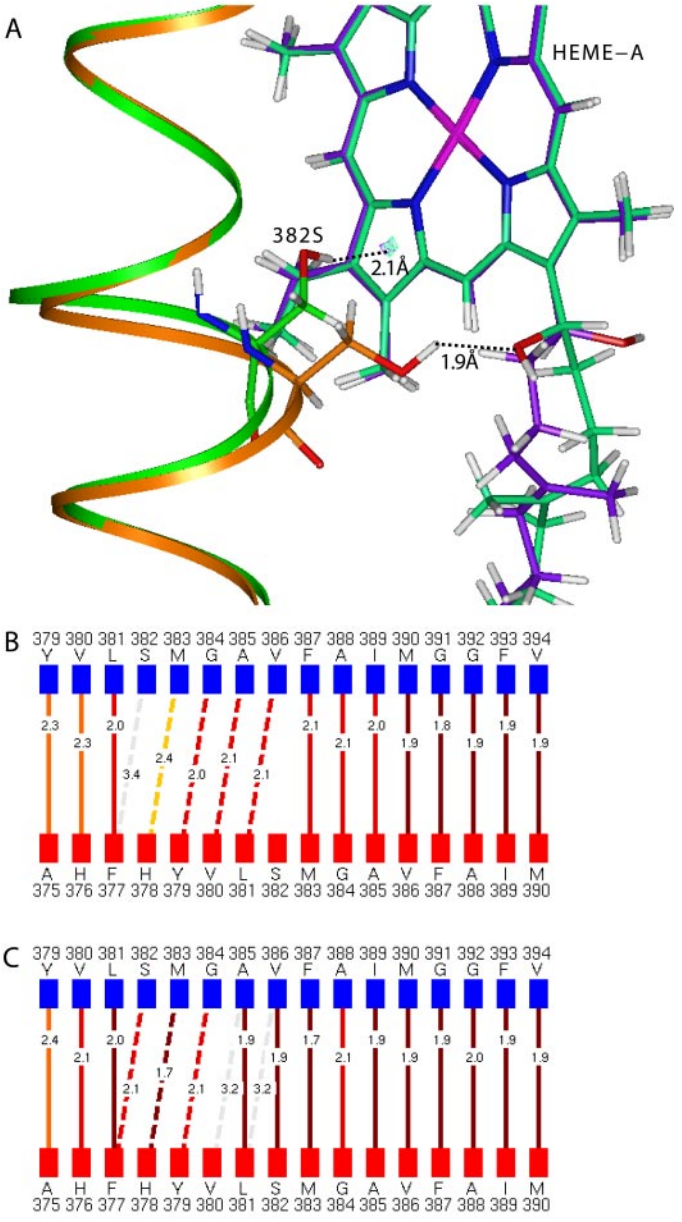

Fig. 7. Redox-dependent alteration in a wide turn from a W_2 to W_3 subclass. A, helical path of the oxidized (green) and reduced (orange) helix 10 (A chain of BCCO) showing W_3 and W_2 configurations, respectively, and associated with different rotameric conformations of Ser382. The different rotamers allow Ser382:Hγ to act as an H-bond donor for binding to a pyrrole ring on heme A or to an OH moiety on the tail of heme A. B and C, H-bonding diagrams (see Fig. 3 for details) of the helix in A with Phe387 as the signature residue in the oxidized form (B), and Gly384 as the signature residue in the reduced form (C), which has changed to α-helical structure in the region N-terminal to Ala385 and Val386.

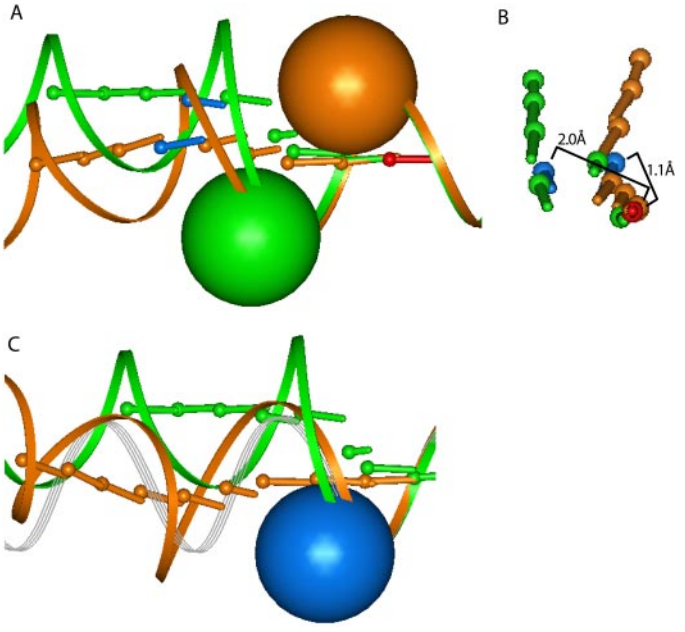

Fig. 8. Modifying effects of nonsignature residues on helical direction. A, differences in the helical axis vectors for W_1 wide turn-containing helices with proline or leucine at the S_{-2} position and threonine or proline, respectively, at the signature residue position. Green, sensory rhodopsin II (SR2), helix 5; orange, *E. coli* Acrb multidrug efflux pump, helix 6. The effective size of the pyrrolidine rings is indicated by the green and orange balls. With proline at the S_0 position (orange), the N-terminal helical path moves out and around the ring with the helical path bending away. Proline at the S_{-2} position (green) has the N-terminal path unwinding to place the ring beyond the helical path. B, the extent of the displacement in A, is shown by the 2.0-Å lateral shift (SR2) in the axis vector (blue) of the S_{-5} segment N-terminal to the reference segment (red). By comparison, the lateral displacement of a proline-induced W_1 wide turn lacking a prolyl residue at the S_{-2} position is only 1.1 Å. C, comparison of the effects of a proline at the S_0 and S_{-2} positions on helical structure. The SR2 helix above is shown in green. The W_1 wide turn in helix 6 of the *E. coli* Acrb multidrug efflux pump is shown in orange, and the path of an α-helix is shown in gray. The structures are aligned with the prolines superimposed and indicated by the blue ball.

orients the carbonyl bond of Ala168 (the residue equivalent to Thr164 in the β_2-AR) away from TM V (Supplemental Fig. 6).

In terms of the W_2 versus W_3 wide-turn difference in TM V of rhodopsin and the β_2-AR, this changes the shape of the transmembrane domain containing these noncanonical regions to alter the positioning and orientation of residues N-terminal to the signature residue, including not only Ser 203 at the S_{-8} position, but Ser207 at the S_{-4} position. Like Ser203, Ser207 is also involved in ligand binding (in this instance via an H-bond interaction with the catechol ring *p*-hydroxyl) and in receptor activation (Strader et al., 1989, Liapakis et al., 2000). Thus, in the absence of a crystal structure for the β_2-AR, it is evident that modeling its binding pocket based on the rhodopsins crystal structure would malposition this critical pair of serine residues, even if the same rotamer positions were maintained as those for Met207 and His211—the rhodopsin TM V residues equivalent to Ser203 and Ser207 in the β_2-AR, respectively.

Conclusion

Using methods to characterize noncanonical regions in transmembrane helices on a reside-to-residue basis, we have identified three different classes of wide turns based on $C\alpha_i \rightarrow C\alpha_x$ distance difference profiles and the number and position of potential π H-bonds. We also show that wide turns result from a series of discrete changes over a number of residues, equivalent to either the widening of a turn or an unwinding of the helix. The path of the helical axis vectors indicates that for proline-induced wide turns, the helix bends around the proline instead of away from the proline, as occurs with tight turns and kinks. The structure of the wide turn introduces flexibility in the helix, which affords unique opportunities for interactions with adjacent helices. With the tools developed, we can more accurately define helical structure and determine the effect of side-chain rotamer conformations, thus bringing us closer to being able to predict with greater accuracy, secondary and, to some degree, even tertiary structure, from primary sequence.

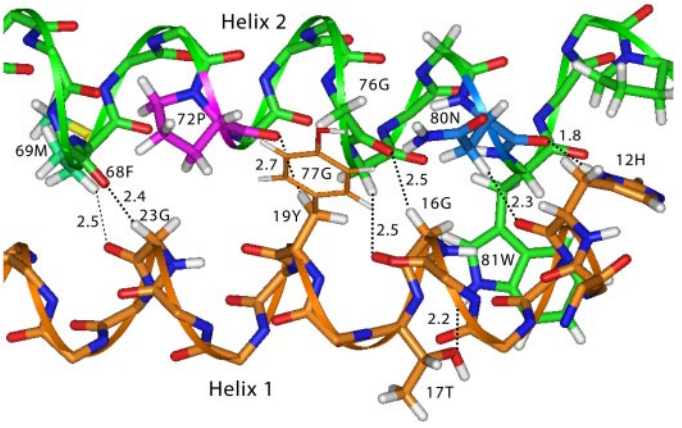

Fig. 9. Multiple interhelical interactions made possible by the presence of wide turns and glycyl residues in adjacent transmembrane helices. Multiple backbone-to-backbone C-H···O H-bonds (dashed lines) between helices 1 (orange) and 2 (green) of the A chain of BCCO are shown. Helix 1 contains a glycine (Gly23) that interacts with Phe68 located on a W_3 wide turn in helix 2 induced by Pro72. Helix 1 also contains another glycine (Gly16) that interacts with both Gly76 and Gly77 located on another helix 2 W_3 wide turn induced by Asn80. In addition, backbone-to-side chain interhelical H-bonds are evident between His12:O and Asn80:Hβ1 (2.3Å), Gly23:O and Met69:Hγ2 (2.5Å), Pro72:O and Tyr19:Hβ1 (2.7Å), and Asn80:O and His12:Hδ1 (1.8Å). An additional side chain-to-side chain H-bond occurs between Thr17:O and Trp81:Hε1 (2.2Å). The intrahelical H-bond, Gly76:O→Asn80:Hβ2 orients the Asn80 side chain, enabling the interhelical H-bond Asn80:O→His12:Hδ1 to form.

Acknowledgments

We are most grateful to Drs. Merridee Wouters, Siiri Iismaa and Daniela Stock for reading the manuscript and for critical input.

References

Aqvist J (1986) A simple way to calculate the axis of an α-helix. *Comput Chem* **10:**97–99.
Bansal M, Kumar S, and Velavan R (2000) HELANAL: a program to characterize helix geometry in proteins. *J Biomol Struct Dyn* **17:**811–819.
Barlow DJ and Thornton JM (1988) Helix geometry in proteins. *J Mol Biol* **201:**601–619.
Berman HM, Westbrook J, Feng Z, Gilliland G, Bhat TN, Weissig H, Shindyalov IN, and Bourne PE (2000) The Protein Data Bank. *Nucleic Acids Res* **28:**235–242.
Bright JN and Sansom MSP (2003) The flexing/twirling helix: exploring the flexibility about molecular hinges formed by proline and glycine motifs in transmembrane helices. *J Phys Chem B* **107:**627–636.
Cartailler JP and Luecke H (2004) Structural and functional characterization of π-bulges and other short intrahelical deformations. *Structure* **12:**133–144.
Cherezov V, Rosenbaum DM, Hanson MA, Rasmussen SG, Thian FS, Kobilka TS, Choi HJ, Kuhn P, Weis WI, Kobilka BK, et al. (2007) High-resolution crystal structure of an engineered human beta-2 G protein-coupled receptor. *Science* **318:**1258–1265.
Christopher JA, Swanson R, and Baldwin TO (1996) Algorithms for finding the axis of a helix: fast rotational and parametric least-squares methods. *Comput Chem* **20:**339–345.
Cogdell RJ, Gall A, and Kohler J (2006) The architecture and function of the light-harvesting apparatus of purple bacteria: from single molecules to in vivo membranes. *Q Rev Biophys* **39:**227–234.
Cordes FS, Bright JN, and Sansom MSP (2002) Proline-induced distortions of transmembrane helices. *J Mol Biol* **323:**951–960.
Desiraju G and Steiner T (1999) Archetypes of the weak hydrogen bond—C–H···O and C–H···N interactions in organic and organometallic systems, in *The Weak Hydrogen Bond in Structural Chemistry and Biology*, pp 29–121, Oxford University Press, Oxford, UK.
Dunbrack RL Jr and Cohen FE (1997) Bayesian statistical analysis of protein sidechain rotamer preferences. *Protein Sci* **6:**1661–1681.
Fodje MN and Al-Karadaghi S (2002) Occurrence, conformational features and amino acid propensities for the pi-helix. *Protein Eng* **15:**353–358.
Frishman D and Argos P (1995) Knowledge-based protein secondary structure assignment. *Proteins* **23:**566–579.
Kabasch W and Sander C (1983) Dictionary of protein secondary structure: pattern recognition of hydrogen-bonded and geometrical features. *Biopolymers* **22:**2577–2637.
Kim S, Jeon T-J, Oberai A, Yang D, Schmidt JJ, and Bowie JU (2005) Transmembrane glycine zippers: Physiological and pathological roles in membrane proteins. *Proc Natl Acad Sci U S A* **102:**14278–14283.
Labesse G, Colloc'h N, Pothier J, and Mornon JP (1997) P-SEA: a new efficient assignment of secondary structure from C alpha trace of proteins. *Comput Appl Biosci* **13:**291–295.
Liapakis G, Ballesteros JA, Papachristou S, Chan WC, Chen X, Javitch JA (2000) The forgotten serines. A critical role for Ser-203$^{5.42}$ in ligand binding to and activation of the β2-adrenergic receptor. *J Biol Chem* **275:**37779–37788.
Lopera JA, Sturgis JN, and Duneau JP (2005) Ptuba: a tool for the visualization of helix surfaces in proteins. *J Mol Graph Model* **23:**305–315.
Lovell SC, Davis IW, Arendall WB 3rd, de Bakker PI, Word JM, Prisant MG, Richardson JS, and Richardson DC (2003) Structure validation by Cα geometry: ϕ, ψ and Cβ deviation. *Proteins* **50:**437–450.
Lovell SC, Word JM, Richardson JS, and Richardson DC (2000) The penultimate rotamer library. *Proteins* **40:**389–408.
MacKenzie KR, Prestegard JH, and Engelman DM (1997) A transmembrane helix dimer: structure and implications. *Science* **276:**131–133.
Mohapatra PK, Khamari A, and Raval MK (2004) A method for structural analysis of α-helices of membrane proteins. *J Mol Model* **10:**393–398.
Muramoto K, Hirata K, Shinzawa-Itoh K, Yoko-O S, Yamashita E, Aoyama H, Tsukihara T, and Yoshikawa S (2007) A histidine residue acting as a controlling site for dioxygen reduction and proton pumping by cytochrome c oxidase. *Proc Natl Acad Sci U S A* **104:**7881–7886.
Nakamichi H and Okada T (2006) Local peptide movement in the photoreaction intermediate of rhodopsin. *Proc Natl Acad Sci U S A* **103:**12729–12734.
Richards FM and Kundrot CE (1988) Identification of structural motifs from protein coordinate data: secondary structure and first-level supersecondary structure. *Proteins* **3:**71–84.
Riek RP, Rigoutsos I, Novotny J, and Graham RM (2001) Non-α-helical elements modulate polytopic membrane protein architecture. *J Mol Biol* **306:**349–362.
Rigoutsos I, Riek P, Graham RM, and Novotny J (2003) Structural details (kinks and non-alpha conformations) in transmembrane helices are intrahelically determined and can be predicted by sequence pattern descriptors. *Nucleic Acids Res* **31:**4625–4631.

Russ WP and Engelman DM (2000) The GxxxG motif: a framework for transmembrane helix-helix association. *J Mol Biol* **296:**911–919.
Scheiner S, Kat T, and Gu Y (2001) Strength of the Cα H·O hydrogen bond of amino acid residues. *J Biol Chem* **276:**9832–9837.
Senes A, Engel DE, and DeGrado WF (2004) Folding of helical membrane proteins: the role of polar, GxxxG-like and proline motifs. *Curr Opin Struct Biol* **14:**465–479.
Senes A, Gerstein M, and Engelman DM (2000) Statistical analysis of amino acid patterns in transmembrane helices: the GxxxG motif occurs frequently and in association with beta-branched residues at neighboring positions. *J Mol Biol* **296:**921–936.
Senes A, Ubarretxena-Belandia I, and Engelman DM (2001) The Cα-H.O hydrogen bond: A determinant of stability and specificity in transmembrane helix interactions. *Proc Natl Acad Sci U S A* **98:**9056–9061.
Strader CD, Candelore MR, Hill WS, Sigal IS, and Dixon RA (1989) Identification of two serine residues involved in agonist activation of the β-adrenergic receptor. *J Biol Chem* **264:**13572–13578.
Sugeta H and Miyazawa T (1967) General method for calculating helical parameters of polymer chains from bond lengths, bond angles and internal-rotation angles. *Biopolymers* **5:**673–679.
Tsukihara T, Shimokata K, Katayama Y, Shimada H, Muramoto K, Aoyama H, Mochizuki M, Shinzawa-Itoh K, Yamashita E, Yao M, et al. (2003) The low-spin heme of cytochrome c oxidase as the driving element of the proton-pumping process. *Proc Natl Acad Sci U S A* **100:**15304–15309.
Tunnicliffe RB, Ratcliffe EC, Hunter CN, and Williamson MP (2006) The solution structure of the PufX polypeptide from *Rhodobacter sphaeroides*. *FEBS Lett* **580:**6967–6971.
Vargas R, Garza J, Dixon DA, and Hay BP (2000) How strong is the Cα-H·O=C hydrogen bond? *J Am Chem Soc* **122:**4750–4755.
Visiers I, Braunheim BB, and Weinstein H (2000) Prokink: a protocol for numerical evaluation of helix distortions by proline. *Protein Engineering* **13:**603–606.
Weaver TM (2000) The pi-helix translates structure into function. *Protein Sci* **9:**201–206.

Address correspondence to: Dr. Robert M. Graham, 384 Victoria Street, Darlinghurst, NSW 2010, Australia. E-mail: b.graham@victorchang.edu.au